Optimization of Image Reconstruction Method of Cerebral Blood Flow Perfusion Imaging with Digital CZT SPECT

Yaqian Zhou
Tianjin Medical University General Hospital https://orcid.org/0000-0001-9235-5973
Shen Wang
Tianjin Medical University General Hospital
Peng Wang
Tianjin Medical University General Hospital
Ning Li
Tianjin Medical University General Hospital
Ruixin Wu
Tianjin Medical University General Hospital
Zhongying Rui
Tianjin Medical University General Hospital
Xuan Wang
Tianjin Medical University General Hospital
Qiang Jia
Tianjin Medical University General Hospital
Wei Zheng (zhengw@tmu.edu.cn)
Tianjin Medical University General Hospital https://orcid.org/0000-0003-1206-9243

Original research

Keywords: CZT SPECT, FBP, OSEM, Butterworth filter, Gauss filter, Cerebral blood flow perfusion imaging

Posted Date: January 15th, 2021

DOI: https://doi.org/10.21203/rs.3.rs-144249/v1

Version of Record: A version of this preprint was published at Nuclear Medicine Communications on January 31st, 2022. See the published version at https://doi.org/10.1097/MNM.0000000000001540.

Abstract

Purpose: To evaluate the effects of filtered back projection (FBP), ordered subset expectation maximisation (OSEM), and different filters on cadmium zinc telluride single photon emission computed tomography (CZT SPECT) cerebral blood perfusion image quality to optimise the image reconstruction method.

Methods: Jaszczak phantom and patients with clinical cerebral ischemia were selected as study subjects. Under routine clinical conditions, tomographic imaging was performed on the phantom and patients with clinical cerebral ischemia. Image processing included image reconstruction using filtered back projection with Chang's attenuation correction ($FBP_{ChangAC}$) and OSEM algorithm with CT-based attenuation correction (CTAC), scatter correction (SC), resolution recovery (RR) ($OSEM_{CTAC\text{-}SC\text{-}RR}$), and the filtering method used Butterworth (Bw) and Gauss (Gs) filters. Visual and semi-quantitative parameters (integral uniformity, root mean square noise (RMS noise), and contrast and contrast-to-noise ratio (CNR)) were used to evaluate image quality to optimise image reconstruction parameters. One-way and two-way ANOVA were used to process phantom and clinical data.

Results: In the tomographic images of phantom and brain imaging of patients, FBP+Bw had the best uniformity and the lowest noise level, while OSEM+Bw had the best contrast. Semi-quantitative analysis showed that the integral uniformity of FBP+Bw was significantly higher than that of OSEM+Bw and OSEM+Gs ($p < 0.05$), and that the RMS noise of FBP+Bw was significantly lower than that of OSEM+Bw and OSEM+Gs ($p < 0.001$). The contrast of FBP+Bw and OSEM+Bw in the cold sphere diameter ≥ 2 cm group was significantly higher than that of OSEM+Gs ($p < 0.001$), while the CNR of FBP+Bw was significantly higher than that of OSEM+Bw and OSEM+Gs ($p < 0.001$) ; the contrast of OSEM+Bw cold sphere diameter < 2 cm was significantly higher than that of FBP+Bw ($p < 0.01$). The semi-quantitative analysis results of the patient's cerebral perfusion tomography were consistent with the model.

Conclusion: In CZT SPECT cerebral blood flow perfusion imaging, images with lesion sizes greater than 2 cm were suitable for FBP+Bw (fc=0.40, n=10), and the image with lesion size less than 2 cm was suitable for OSEM+Bw (EM=60, fc=0.45, n=10). The reconstruction method of OSEM+Gs (EM=80, full width at half maximum [FWHM]=3.25) was not suitable for cerebral blood perfusion imaging.

Background

As a common clinical neurosurgical disease, ischemic cerebrovascular disease has high disability and mortality rates worldwide. With an increasing aging population, the incidence of this disease has been increasing year by year, and it has become a public health concern threatening human health. Cerebral blood perfusion imaging can be used to assess the local cerebral blood flow and cerebrovascular reserve at rest, and it has unique advantages in lesion guidance; prognostic evaluation of many diseases such as cerebral infarction, transient ischemic attack (TIA), epilepsy, and other ischemic lesions; and normal brain function research [1–3].

With the development of imaging technology, especially functional imaging, single-photon emission computed tomography (SPECT) has played an increasingly important role in the localisation and diagnosis of ischemic cerebrovascular diseases. In recent years, the development of digital universal tellurium-zinc-cadmium (CZT) cameras has promoted new advances in SPECT imaging technology. When compared to SPECT equipped with a traditional sodium iodide detector (NaI SPECT), SPECT equipped with a CZT semiconductor detector (CZT SPECT) provides better image quality, and the spatial resolution, energy resolution, and contrast of CZT SPECT images have significantly improved [4–6].

Currently, CZT-based cameras can provide better image quality than NaI-based cameras, but the image processing method for cerebral perfusion imaging still adopts the traditional method of NaI SPECT. Therefore, we explored the effects of different reconstruction algorithms and filter parameters on CZT SPECT cerebral blood flow perfusion image quality in phantom and clinical cases, to optimise the image reconstruction parameters of CZT SPECT imaging so as to better assist clinical diagnosis.

Materials And Methods

Instruments and equipment

The acquisition instrument was Discovery NM/CT870 (GE Healthcare, USA), which was composed of two CZT semiconductor detectors and could be arranged in multiple angles. Each detector consisted of 10 × 13 CZT modules, with each module including 16 × 16 CZT pixel units, and was equipped with wide-energy high-resolution collimators aligned with the pixel array. The image was processed using a Xeleris 4.0 workstation (GE Healthcare, USA).

The phantom used was the Jaszczak phantom (Deluxe ECT Phantom, Model ECT/DLX/P, Data Spectrum Corporation, USA), which was divided into a uniform area (background area) and a cold area (defect area). There were no plug-ins in the uniform zone, and there were six solid ball plug-ins in the cold zone (their diameters were 31.8, 25.4, 19.1, 15.9, 12.7, and 9.5 mm).

The background area of the phantom was filled with water and injected with $^{99m}TCO_4^-$solution 480 MBq (specific activity: 0.069 MBq/mL). After full concussion, the phantom was placed for 2 h, so that the solution in the phantom was fully mixed.

Phantom imaging

The phantom was placed in the centre of the probe's field of view, where the axis was parallel to the long axis of the scanning bed. The image acquisition scheme simulated the clinical acquisition method. The SPECT parameters used were automatic human body contour technology, the acquisition matrix was 128 × 128, the pixel size was 3.32 mm, the zoom was 1.33, the acquisition speed was 20 s/frame, with a total of 120 frames, with the light peak of ^{99m}Tc as the centre, and the energy window was 140 KVp ± 7.5%. The CT scanning parameters were as follows: tube voltage was 120 KVp; tube current, 150 mA; layer

thickness, 2.5 mm; and pitch, 0.875:1. The phantom imaging experiments were repeated five times, and all the data were studied by taking the average of the five experiments.

Image reconstruction

Phantom images reconstruction

In CZT SPECT cerebral blood flow perfusion imaging, the main methods for brain imaging image reconstruction are filtered back projection (FBP) reconstruction with Chang attenuation correction (ChangAC) [5] and conventional ordered subset expectation maximisation (OSEM) reconstruction [6]. The most commonly used filters for cerebral blood flow perfusion imaging are the Butterworth filter and Gauss filter [7–9]. Therefore, three image reconstruction methods commonly used in clinics were used to process phantom images:

Combination 1: FBP reconstruction + Butterworth post-filtering (later replaced by FBP + Bw)

The phantom image was reconstructed using the FBP algorithm with ChangAC ($FBP_{ChangAC}$), and the $FBP_{ChangAC}$ image was post-filtered using a Butterworth filter. The threshold of ChangAC was 10 and the attenuation coefficient μ was 0.12 cm^{-1}. First, different cut-off frequency (fc) values were selected (0.30, 0.35, 0.40, 0.45, 0.50, 0.55) under the condition that the order(n) = 10 (manufacturer's recommended reference value) remained unchanged. Then, according to the values of integral uniformity, root mean square noise (RMS noise), contrast, and contrast-to-noise ratio (CNR), the optimal value of fc was determined to remain unchanged, and different n values (5, 10, 15, 20, 25, 30) were selected, and different filter parameters were used for post-processing of $FBP_{ChangAC}$ images.

Combination 2: OSEM reconstruction + Butterworth post-filtering (later replaced by OSEM + Bw)

Subset and iteration times had the same effects on image improvement; therefore, we could define a number of expectation maximisation-equivalent iterations (EM), which represented the product of the subset and the number of iterations [7, 10].

The phantom image was reconstructed using the OSEM algorithm ($OSEM_{CTAC-SC-RR}$) including CT-based attenuation correction (CTAC), scatter correction (SC), and resolution recovery (RR). The Butterworth filter was used to post-filter the $OSEM_{CTAC-SC-RR}$ image. First, the filter parameters were fixed (referred to combination 1: fc = 0.40 ~ 0.45, n = 10); then, the subset of $OSEM_{CTAC-SC-RR}$ was fixed at 10 and the number of iterations were 2, 4, 6, 8, 10, and 12 to determine the optimal value of EM. The optimal parameters of the filter were verified; the selection of filter parameters referred to the method of combination 1. First, n = 10 was fixed, different fc values were selected (0.30, 0.35, 0.40, 0.45, 0.50, 0.55), and then the optimal value of fc was determined, different n values were chosen (5, 10, 15, 20, 25, 30), and the best filtering parameters in the OSEM + Bw were determined.

Combination 3: OSEM reconstruction + Gauss post-filtering (later replaced by OSEM + Gs)

The $OSEM_{CTAC-SC-RR}$ was used to reconstruct the image, the EM value was fixed at 60 (referred to the result of combination 2), and a Gauss filter was used (full width at half maximum [FWHM] = 2.50, 2.75, 3.00, 3.25, 3.50, 3.75 mm) to smooth the $OSEM_{CTAC-SC-RR}$ image, to determine the best parameters of the Gauss filter. Then, the filter parameters were fixed to verify the best EM value of OSEM reconstruction in combination 3. With reference to the method of combination 2, the subset of $OSEM_{CTAC-SC-RR}$ was fixed at 10, and the number of iterations were 2, 4, 6, 8, 10, and 12 to determine the optimal value of EM.

Semi-quantitative analysis

To more accurately compare the phantom image quality after different processing, the phantom image quality was quantitatively evaluated by calculating integral uniformity, RMS noise, and contrast[11].

Uniformity and noise

Five 15×15-pixel square regions of interest (ROIs) were drawn at different positions on the transverse of the uniform part of the phantom to record the average, maximum, minimum, and standard deviation of the radioactivity count in each ROI, and the formula calculation was carried out after taking the average of each value, such as formulas (1) and (2).

$$\text{Integral uniformity } (\%) = \frac{(\text{max count} - \text{min count})}{\text{max count} + \text{min count}} \times 100\% \quad (1)$$

$$RMS\ \ noise(\%) = \frac{\text{standard deviation}}{\text{mean count}} \times 100\% \quad (2)$$

Contrast

The most obvious transverse of the cold spheres was selected, the minimum value of the radioactivity count in each cold sphere of the selected layer was determined, and five 15×15-pixel square ROIs were drawn to record the average radioactivity count value in different positions of the uniform background of the phantom, such as formula (3).

$$Contrast = \frac{\text{mean count}_{\text{background}} - \text{min count}_{\text{coldsphere}}}{\text{mean count}_{\text{background}}} \quad (3)$$

CNR

To objectively compare the effects of different processing combinations on image quality, the CNR of different spheres was calculated, such as formula (4). CNR was not a standard parameter but could be expressed by the quotient of contrast and noise. When further increasing the number of EM caused the

CNR of the visible minimum sphere to increase by less than 5% [12], it was defined as the best equivalent number of iterations of the OSEM reconstruction algorithm.

$$CNR = \frac{\text{mean count}_{\text{coldsphere}} - \text{mean count}_{\text{background}}}{\text{standard deviation}_{\text{background}}} \quad (4)$$

Clinical image verification

Different reconstruction methods were used to evaluate the effect on the image quality of lesions of different sizes. The clinical images of 20 patients with abnormal cerebral blood perfusion were selected for verification: (1) all cases were composed of patients with cerebral blood perfusion defect or relative decrease diagnosed by doctors, (2) the lesion size of 10 patients was less than 2 cm, and the lesion size of the other 10 patients was ≥ 2 cm. The best parameters of the three reconstruction methods (FBP + Bw, OSEM + Bw, and OSEM + Gs) were used to post-process the CZT SPECT images of all patients.

According to the semi-quantitative analysis method of the model study, the integral uniformity, RMS noise, contrast, and CNR of lesions were calculated to evaluate the image quality. Two ROIs of the same size (the same size as the focus) were drawn on the clinical image: one on the focus (cold area) and one on the healthy tissue near the lesion (background area).

Statistical analysis

Data were presented as the mean ± standard deviation (x ± s). The data were analysed using SPSS 26.0 software, one-way ANOVA and two-way ANOVA were used for phantom data, one-way ANOVA were used for clinical data, and pairwise comparison were used LSD method. Each experiment was performed in quintuplicate unless otherwise stated. A p-value < 0.05 indicated that the difference was statistically significant.

Results

Phantom image quality

Combination 1: FBP + Bw

With an increase in the n value, the contrast and CNR of the image increased, while the uniformity and noise decreased and converged uniformly when n ≥ 10. With an increase in the fc value, the contrast of the image increased, the CNR decreased, the uniformity and noise of the image increased, and the contrast and CNR decreased with decreasing diameter of the cold spheres, as shown in Fig. 1A.

When fc = 0.30 ~ 0.35, the image was too smooth and the contrast was poor. With an increase in the fc value, the uniformity and noise of the image increased (Fig. 2A), the CNR of the image decreased (Fig. 4A), and the contrast increased (Fig. 3A), which could distinguish smaller cold spheres, while the contrast and CNR decreased with decreasing diameter of the cold ball. When the fc value was greater

than 0.5, the image uniformity was poor and the noise level increased significantly. When fc = 0.40 ~ 0.45, the cold sphere contrast was better and the image quality was relatively good.

When fc = 0.40 ~ 0.45, n < 10, the uniformity of the image was poor, and the noise was obvious. With an increase in the n value, the contrast (Fig. 3B, 3C) and CNR (Fig. 4B, 3C) of the image increased, while the uniformity and noise decreased (Fig. 2B) and converged uniformly when n ≥ 10. When n = 10 ~ 30, the resolution of the image was the best.

Combination 2: OSEM + Bw

With the increase in EM, the contrast of the image increased, the CNR decreased, the noise of the image also increased, and the uniformity of the image became worse, as shown in Fig. 1B.

When EM < 60, the image was too smooth, and the small diameter of the cold sphere was unclear; when EM ≥ 60, the image resolution was high, but the noise level increased (Fig. 2C). With the increase in EM, the image contrast (Fig. 3D, 3E) and CNR (Fig. 4D, 4E) increased, and when EM ≥ 60, the cold sphere contrast of the image and the growth of CNR plateaued. When EM = 60, the CNR of the smallest cold sphere that could be recognised increased by less than 5%.

The verification of the best parameters of the Butterworth filter showed that when EM = 60 was the same as the result of combination 1, the overall quality of the image was the best when the filtering parameters were ‘fc = 0.40 ~ 0.45, n = 10 ~ 30’; when the fc value was too low, the image was too smooth and the contrast was poor, while when the fc value was too high, the image uniformity became worse and the noise level increased significantly. Similarly, the uniformity of the image with n < 10 was poor, and the noise was obvious. With an increase in the n value, the contrast and CNR of the image increased, but the uniformity and noise decreased and converged uniformly when n ≥ 10.

In addition, for different Bw parameters (‘fc = 0.40, n = 10’ and ‘fc = 0.45, n = 10’) under OSEM (EM = 60) reconstruction, it could be concluded that the CNR value of fc = 0.45 was larger than that of fc = 0.40, especially for cold spheres with small diameters.

Combination 3: OSEM + Gs

With an increase in the FWHM value, the uniformity and noise of the image decreased, and the image tended to be smooth. Additionally, the contrast of the image also decreased, and some details of the image were lost, as shown in Fig. 1C.

Under the condition of constant EM = 60, when the FWHM < 3.00 of the Gs parameter, the image uniformity was worse and the noise was greater; with an increase in the FWHM value, the image uniformity was better, and the noise was reduced (Fig. 2D). However, when the FWHM > 3.25, the image was too smooth, the cold sphere contrast was poor (Fig. 3F), and the CNR value was also reduced (Fig. 4F). Therefore, when FWHM = 3.0 ~ 3.25, the overall quality of the image was better. The optimal EM value was verified in the OSEM + Gs: when EM = 80, further increased the EM, the CNR value of the minimum cold sphere that could be identified was less than 5%.

Among the three processing combinations, from the point of view of uniformity, noise, and CNR, the image quality of FBP + Bw was significantly better than that of OSEM + Bw and OSEM + Gs. From the point of view of contrast, the image contrast of OSEM + Bw was significantly better than that of FBP + Bw and OSEM + Gs. Therefore, the semi-quantitative parameters obtained from the visual analysis were as follows: FBP + Bw (fc = 0.40 ~ 0.45, n = 10), OSEM + Bw (EM = 60, fc = 0.40 ~ 0.45, n = 10), and OSEM + Gs (EM = 80, FWHM = 3.00 ~ 3.25) for further optimization.

Results of semi-quantitative analysis of phantom

The integral uniformity of FBP + Bw (fc = 0.40, n = 10) (9.68 ± 1.16) was the best and was significantly better than that of OSEM + Bw (16.50 ± 3.10 ~ 17.95 ± 2.89) and OSEM + Gs (14.40 ± 1.23 ~ 15.31 ± 1.50) ($p < 0.05$) (Fig. 5). Additionally, FBP + Bw (fc = 0.40, n = 10) (4.03 ± 0.37) had the lowest RMS noise, significantly better than that of OSEM + Bw (7.12 ± 1.21 ~ 7.52 ± 1.01) and OSEM + Gs (6.17 ± 0.76 ~ 6.43 ± 0.73) ($p < 0.001$) (Fig. 5). However, the contrast of OSEM + Bw (EM = 60, fc = 0.45, n = 10) (0.66 ± 0.26) was the highest and was significantly higher than that of FBP + Bw (0.55 ± 0.30 ~ 0.58 ± 0.30) and OSEM + Gs (0.53 ± 0.22 ~ 0.55 ± 0.22) ($p < 0.001$) (Fig. 6A). The CNR of FBP + Bw (fc = 0.40, n = 10) (13.60 ± 7.53) was the highest and was significantly higher than that of OSEM + Bw (9.24 ± 4.28 ~ 8.90 ± 3.71) and OSEM + Gs (8.76 ± 3.71 ~ 8.68 ± 3.53) ($p < 0.001$) (Fig. 6B).

Comparison of semi-quantitative analysis results of cold spheres of different sizes in the phantom

From the phantom images, there were differences in the display of cold spheres of different sizes using different methods. Therefore, the five identifiable cold spheres were divided into two groups (diameter ≥ 2 cm group: 31.8 and 25.4 mm cold spheres, diameter < 2 cm group: 19.1, 15.4, and 12.7 mm cold spheres), and the differences were analysed using three reconstruction methods: FBP + Bw (fc = 0.40, n = 10), OSEM + Bw (EM = 60, fc = 0.45,n = 10), and OSEM + Gs (EM = 80, FWHM = 3.25) (Fig. 7A,7B)

For the 31.8 mm cold sphere (Fig. 7A), the contrast of FBP + Bw (0.97 ± 0.02) and OSEM + Bw (0.95 ± 0.03) were significantly higher than that of OSEM + Gs (0.82 ± 0.02) (p values were all < 0.001), but there was no significant difference between FBP + Bw and OSEM + Bw ($p > 0.05$). In addition, the CNR value of FBP + Bw (23.67 ± 3.03) was higher than that of OSEM + Bw (12.79 ± 1.56) and OSEM + Gs (13.43 ± 1.55) ($p < 0.001$), and there was no significant difference in CNR between OSEM and OSEM ($p > 0.05$). Furthermore, the difference in the diameter of the 25.4 mm cold sphere under the three reconstruction methods was also analysed, and it was found that the contrast of FBP + Bw (0.77 ± 0.07) was significantly lower than that of OSEM + Bw (0.90 ± 0.03) ($p < 0.05$). The other results were the same as those of the 31.8 mm cold sphere.

For the 12.7 mm cold sphere (Fig. 7B), the contrast of OSEM + Bw (0.29 ± 0.05) was significantly higher than that of FBP + Bw (0.18 ± 0.03) ($p < 0.01$), but there was no significant difference among the other groups ($p > 0.05$). In addition, there was no significant difference in CNR among all combinations ($p > 0.05$). Similarly, the differences in cold spheres with 15.9 mm and 19.1 mm diameters under the three

reconstruction methods were statistically analysed, and the results were similar to those of the 12.7 mm cold sphere.

Clinical case images

Figure 8 shows that the image quality of cerebral perfusion tomography in patients with lesion size ≥ 2 cm was the best under FBP + Bw. Excessive compensation of OSEM + Bw images might have lead to false-negative results, while OSEM + Gs images were too smooth, which was not conducive to clinical diagnosis. In the patients with lesion size < 2 cm, the focus was shown most clearly on OSEM + Bw, followed by FBP + Bw, and the worst on OSEM + Gs.

Semi-quantitative analysis results of clinical images (Table 1)

The average integral uniformity of FBP + Bw (15.19 ± 3.08) in the group with lesion size ≥ 2 cm was significantly better than that of OSEM + Bw (20.96 ± 6.99) and OSEM + Gs (10.65 ± 2.76) (p values were all < 0.05). However, there was no significant difference in contrast and CNR among the three groups (p > 0.05).

The contrast ratio of OSEM + Bw (0.42 ± 0.11) was significantly higher than that of FBP + Bw (0.32 ± 0.12) (p < 0.05) in the group with lesion size < 2 cm, but there was no significant difference among the other groups (p > 0.05). There was no significant difference in uniformity, noise, or CNR among the three groups.

Table 1
Semi-quantitative analysis results of two groups of patient images processed by different reconstruction methods.

Lesion size	Reconstruction method	Integral uniformity (%)	RMS noise (%)	Contrast	CNR
< 2 cm	FBP + Bw	14.05 ± 4.82	7.24 ± 2.15	0.32 ± 0.12*	4.74 ± 2.52
	OSEM + Bw	16.44 ± 7.79	9.11 ± 3.86	0.42 ± 0.11*	5.77 ± 4.10
	OSEM + Gs	15.72 ± 6.66	8.79 ± 3.58	0.38 ± 0.11	5.12 ± 3.30
≥ 2 cm	FBP + Bw	15.19 ± 3.08+	8.04 ± 1.70−	0.49 ± 0.16	6.30 ± 2.20
	OSEM + Bw	20.96 ± 6.99+	10.65 ± 2.76−	0.57 ± 0.19	5.44 ± 1.79
	OSEM + Gs	18.97 ± 6.26	9.49 ± 2.67	0.52 ± 0.18	5.66 ± 1.89
All data are expressed as x ± s.					
*: Indicates that the difference between the two is statistically significant, p = 0.04.					
+: Indicates that the difference between the two is statistically significant, p = 0.032.					
−: Indicates that the difference between the two is statistically significant, p = 0.023.					

Discussion

Different reconstruction algorithms and filters can be used in CZT SPECT imaging to achieve different purposes, such as reducing star artifacts, suppressing noise, and restoring or enhancing signals. FBP is the most widely used reconstruction method in clinical SPECT. It has the advantages of simplicity, rapidity, and high computational efficiency. It included two steps: filtering of data and back-projection of the filtered data [13]. Chang AC has been the most commonly used AC in FBP reconstruction. The iterative method is a step-by-step mathematical calculation method, which first sets all the pixel values in the image to be reconstructed to the same value, and then compares the projection values of the image in all directions with the actual collected projection values. All pixel values of the image are recalculated, and the image is updated according to their differences. Then, the projection value of each point is calculated for the updated image. The above steps are repeated, and when the difference between the projection value obtained from the image and the actual projection value are small to a certain extent, the iterative process ends and the image reconstruction is completed [13]. Among them, OSEM was the most commonly used iterative reconstruction method, which greatly reduced the number of iterations required. The OSEM-used RR method has been shown to improve the spatial resolution, contrast, and quantitative

accuracy of cerebral perfusion SPECT [14, 15]. CTAC has been considered to be the most accurate AC method for measuring radioactivity in real areas [16].

The filter was used to reduce the noise of the image and also compensate for the loss of details in the image. The Butterworth filter was a low-pass filter that allowed low frequencies to remain unchanged and prevented high frequencies from passing through. It had two parameters: the “cutoff frequency(fc)” and the “order(n)”. The fc defined the frequency above which the noise was eliminated. n controls the slope of the filter function and characterises the steepness of the roll-off. Because the Butterworth filter could not only change the cut-off frequency, but also change the steepness of the roll, it could not only smooth the noise, but also maintain the image resolution. Among them, the selection of fc was of great significance in reducing noise and retaining image details [17]. A higher fc value would improve the spatial resolution and retain more details, while a lower fc value could enhance the smoothing effect of the images but reduced the contrast of images. A Gauss filter is a kind of linear smoothing filter, which is very effective in eliminating Gaussian noise with normal distribution, that is suitable for image smoothing denoising of uniform tissue imaging, such as brain tissue. The width of the Gaussian filter was represented by FWHM in the image processing software, and FWHM determined the smoothness of the image. The larger the FWHM, the wider the frequency band of the Gauss filter and the better the smoothness [18]. By adjusting the FWHM parameter, we could make a compromise between the excessive blur (over-smoothing) of image features and the existence of too much noise and unnecessary details (under-smoothing) in the images. For a given image reconstruction task, the choice of filter was usually a balance between noise reduction and contrast enhancement [9].

Clinically, different reconstruction algorithms and filters are often selected for different diseases in order to achieve the best quality of tomographic images. The SPECT images of patients with brain defects such as cerebral infarction and epilepsy [19] usually used the reconstruction methods of FBP + Bw and OSEM + Bw, while for the SPECT images of patients with Parkinson's disease, the reconstruction method of OSEM + Gs was often used [20, 21]. Similarly, different processing parameters could also meet the needs of image reconstruction in different situations. Winz et al. [22] reported that the relatively low filter cut-off frequency in OSEM reconstruction reduced the image quality to some extent, but the resulting low-noise image was beneficial to the definition of the reference area in dopamine transporter imaging and avoided uptake asymmetry in the posterior putamen, which could avoid misdiagnosis as neurodegeneration. In this study, using the reconstruction method of OSEM + Bw and choosing a slightly higher fc value could improve the contrast of small lesions in patients with brain defects and avoid missed diagnosis.

In this study, phantom analysis and clinical verification were performed for cerebral blood flow perfusion tomography imaging. First, in the phantom tomographic images, the integral uniformity, RMS noise, and contrast of FBP + Bw increased with increasing fc value, but CNR decreased with an increase in fc value. This difference was caused by the enhancement of the high-frequency noise. The higher the fc value was, the more high-frequency components were enhanced, which increased the detection of the image and focus edge and also increased the high-frequency noise. Therefore, the smaller the size of the focus to be

resolved, the higher the fc value in order to meet the diagnostic requirements of the image, but not an excessively high fc value because it would lead to excessive amplification of noise and increase of artifacts, affecting image quality. At the same time, the integral uniformity, RMS noise, and CNR of the image increased with an increase in order, but when the n value was greater than 10, the integral uniformity and RMS noise converged uniformly. Therefore, we determined that the best reconstruction parameter of conventional brain imaging was 'fc = 0.40 ~ 0.45, n = 10 ~ 30'. Khorshidi et al. [23] reported that in conventional NaI SPECT studies, the ideal image quality of brain defects could be obtained when the order of Bw was 7 ~ 10 and the cut-off frequency was 0.45 ~ 0.50. This conclusion was similar to the results of this study.

Second, the integral uniformity, RMS noise, and contrast in OSEM + Bw increased with the increase in EM, but CNR decreased with the increase in EM. It might be that with the increase in EM, the effect on image noise exceeded the influence of contrast, but when EM ≥ 60, the contrast and CNR converged uniformly. Compared with FBP + Bw, the best reconstruction parameter of OSEM + Bw was that 'EM = 60, fc = 0.45, and n = 10' was more accurate in the diagnosis of small lesions. Van Laere et al. [24] reported that in traditional NaI SPECT studies, the best processing parameter for normal brain imaging was OSEM (4 iterations, 6 subsets) + Butterworth (fc = 0.40, n = 8).

The integral uniformity and RMS noise in OSEM + Gs decreased with the increase in FWHM, while the contrast increased with the increase in FWHM, and the overall quality of the image was not as good as that of the combination of the other two processes. Lingfeng et al. [18] showed that the pure noise reduction of 3D Gaussian filters in post-filtering would lead to a decrease in image contrast with the reduction of noise. However, in a study by Matsutomo et al. [20] of conventional NaI SPECT, the reconstruction method of OSEM + Gs could improve the performance and image quality of 123I-Nomega-fluoropropyl-2beta-carbomethoxy-3beta-(4-iodophenyl)nortropane (^{123}I-FP-CIT) SPECT dopamine transporter imaging during the 'EM = 90, FWHM = 6.6mm'. Therefore, it was speculated that the reconstruction method of OSEM + Gs in CZT SPECT imaging might be more suitable for ^{123}I-FP-CIT SPECT imaging. This imaging method has been widely used in the diagnosis of Parkinson's disease and Lewy body dementia [21].

In the semi-quantitative analysis of the cold sphere diameter ≥ 2 cm group, the contrast and CNR of FBP + Bw were significantly higher than those of OSEM + Bw and OSEM + Gs ($p > 0.05$). It was suggested that FBP + Bw had higher identifiability of large lesions, so more attention should be paid to the quality of image uniformity and noise in image reconstruction. For the semi-quantitative analysis of cold sphere diameter < 2 cm, the recognisability of FBP + Bw was lower than that of OSEM + Bw; therefore, in the case of small ischemic lesions, the OSEM reconstruction algorithm could increase the contrast between lesions and normal tissue and improve the recognisability of lesions, so as to avoid a missed diagnosis. These results were preliminarily verified in clinical cases of cerebral ischemia in this study.

In the acquisition process of phantom imaging, a narrower energy window (140 KVp ± 7.5%) was used compared with the traditional SPECT (140 KVp ± 10%) because the digital SPECT improved the energy

resolution. In the phantom image, the size of these cold spheres was smaller than the actual size of these cold spheres, especially in the smaller structure (i.e. the solid balls of 19.1 mm, 15.9 mm, 12.7 mm), which was partly due to the influence of partial volume effect (partial-volume effects, PVE). Matsuda et al. [25] reported that SPECT images could reflect not only the loss of brain volume, but also the changes in brain function, and the regional cerebral blood flow (rCBF) could be measured more accurately by using PVE correction in cerebral perfusion SPECT. In addition, in OSEM reconstruction, the visual distortion of circular cold spheres might be caused by the use of the RR algorithm [26].

The limitations of this study are as follows. First, the unexplained radioactive sparse area in the phantom image might be caused by the examination table. Due to the large size of the phantom, it was impossible to use a clinical dedicated headrest. Second, in order to simulate the current clinical acquisition methods, the matrix size was 128×128. If a matrix size of 256×256 was used, a better image spatial resolution could be obtained, which may improve the image quality. Finally, we did not evaluate the impact on image quality and quantisation by the number of subsets, although image quality was generally not affected by the number of subsets [27]. Further research is underway, and we will increase clinical studies to prove the feasibility of different reconstruction methods for different lesion sizes. This result may be helpful in improving the accuracy of clinical diagnosis, especially for some small lesions that are easily missed.

Conclusion

In conclusion, the image of lesion size ≥ 2 cm in CZT SPECT cerebral blood flow perfusion imaging was suitable for FBP + Bw (fc = 0.40, n = 10). The image of lesion size < 2 cm was suitable for OSEM + Bw (EM = 60, fc = 0.45, n = 10), and OSEM + Gs (EM = 80, FWHM = 3.25) was not suitable for cerebral blood flow perfusion imaging.

Abbreviations

ordered subset expectation maximisation (OSEM)

cadmium zinc telluride single photon emission computed tomography (CZT SPECT)

filtered back projection with Chang's attenuation correction ($FBP_{ChangAC}$)

CT-based attenuation correction (CTAC)

scatter correction (SC)

resolution recovery (RR)

Gauss filter (Gs)

Butterworth filter (Bw)

root mean square noise (RMS noise)

contrast and contrast-to-noise ratio (CNR)

expectation maximisation (EM)

123I-Nomega-fluoropropyl-2beta-carbomethoxy-3beta-(4-iodophenyl)nortropane (^{123}I-FP-CIT)

partial-volume effects (PVE)

regional cerebral blood flow (rCBF)

Declarations

Availability of data and materials

All clinical data are from the Nuclear Medicine Department of Tianjin Medical University General Hospital. The datasets used and/or analysed during the current study are available from the corresponding author on reasonable request.

Ethics approval and consent to participate

All procedures performed in studies involving human participants were in accordance with the ethical standards of the institutional and/or national research committee and with the 1964 Helsinki Declaration and its later amendments or comparable ethical standards.

Consent for publication

Not applicable.

Competing interests

The authors declare that they have no conflict of interest.

Funding

This work was supported by the National Natural Science Foundation of China (Grant No. 81601523), Tianjin Health Science and Technology Project (Grant No.ZC20181), Youth Incubation Fund of Tianjin Medical University General Hospital (Grant No.ZYYFY2019027), and Thyroid Research Program of Young and Middle-aged Physicians (Orbital PET/MR imaging of Graves' disease in BALB/ C mice with Graves ophthalmopathy model China Health Promotion Foundation).

Authors' contributions

Y.Q. Zhou participated in the design and coordination of the study, phantom studies for image quality validation, analyzed the results, and helped draft the manuscript; SW and PW led the image acquisition, reconstruction implementation, and optimization; NL led the clinical applications and study design, study support, and statistical analysis of the results; Z.Y Rui and R.X. Wu participated in design and coordination of the study; and WZ participated in the design and coordination of the study, analyzed the results, and helped draft the manuscript. All authors read and approved the final manuscript.

Acknowledgements

Not applicable.

References

1. Fei, P., et al., *The Value of Regional Cerebral Blood Flow SPECT and FDG PET in Operculoinsular Epilepsy.* Clin Nucl Med, 2018. **43**(3): p. e67-e73.
2. Rösner, A., et al., *Assessment of myocardial ischemia by strain dobutamine stress echocardiography and cardiac magnetic resonance perfusion imaging before and after coronary artery bypass grafting.* Echocardiography, 2017. **34**(4): p. 557-566.
3. Nomura, J., et al., *Combination of blood flow asymmetry in the cerebral and cerebellar hemispheres on brain perfusion SPECT predicts 5-year outcome in patients with symptomatic unilateral major cerebral artery occlusion.* Neurol Res, 2014. **36**(3): p. 262-9.
4. Liga, R. and A. Gimelli, *Imaging the heart's brain: Simultaneous innervation/perfusion analysis in the era of new CZT cameras.* J Nucl Cardiol, 2017. **24**(4): p. 1374-1377.
5. Goshen, E., et al., *Feasibility study of a novel general purpose CZT-based digital SPECT camera: initial clinical results.* EJNMMI Phys, 2018. **5**(1): p. 6.
6. Bordonne, M., et al., *Brain perfusion SPECT acquired using a dedicated brain configuration on a 360° whole-body CZT-camera.* J Neuroradiol, 2020. **47**(2): p. 180-181.
7. Brambilla, M., et al., *Characterization of ordered-subsets expectation maximization with 3D post-reconstruction Gauss filtering and comparison with filtered backprojection in 99mTc SPECT.* Ann Nucl Med, 2005. **19**(2): p. 75-82.
8. Dickson, J.C., et al., *The impact of reconstruction method on the quantification of DaTSCAN images.* Eur J Nucl Med Mol Imaging, 2010. **37**(1): p. 23-35.
9. Lyra, M. and A. Ploussi, *Filtering in SPECT Image Reconstruction.* Int J Biomed Imaging, 2011. **2011**: p. 693795.
10. Olsson, A., et al., *Evaluation of reconstruction techniques in regional cerebral blood flow SPECT using trade-off plots: a Monte Carlo study.* Nucl Med Commun, 2007. **28**(9): p. 719-25.
11. Desmonts, C., et al., *Evaluation of a new multipurpose whole-body CzT-based camera: comparison with a dual-head Anger camera and first clinical images.* EJNMMI Phys, 2020. **7**(1): p. 18.

12. Grootjans, W., et al., *Performance of 3DOSEM and MAP algorithms for reconstructing low count SPECT acquisitions.* Z Med Phys, 2016. **26**(4): p. 311-322.
13. Groch, M.W. and W.D. Erwin, *SPECT in the year 2000: basic principles.* J Nucl Med Technol, 2000. **28**(4): p. 233-44.
14. Onishi, H., et al., *Quantitative performance of advanced resolution recovery strategies on SPECT images: evaluation with use of digital phantom models.* Radiol Phys Technol, 2013. **6**(1): p. 42-53.
15. Yokoi, T., H. Shinohara, and H. Onishi, *Performance evaluation of OSEM reconstruction algorithm incorporating three-dimensional distance-dependent resolution compensation for brain SPECT: a simulation study.* Ann Nucl Med, 2002. **16**(1): p. 11-8.
16. Akamatsu, M., et al., *Influences of reconstruction and attenuation correction in brain SPECT images obtained by the hybrid SPECT/CT device: evaluation with a 3-dimensional brain phantom.* Asia Ocean J Nucl Med Biol, 2014. **2**(1): p. 24-9.
17. Lyra, M., et al., *Filters in 2D and 3D Cardiac SPECT Image Processing.* Cardiol Res Pract, 2014. **2014**: p. 963264.
18. Lingfeng, W., et al., *Effect of reconstruction and filtering on kinetic parameter estimation bias and reliability for dynamic SPECT: a simulation study.* IEEE Transactions on Nuclear Science, 2005. **52**(1): p. 69-78.
19. Ben Mahmoud, S., et al., *Localization of temporal epilepsy foci by subtraction ictal perfusion single photon emission computed tomography is enhanced when using 3D-OSEM iterative reconstruction.* Nucl Med Commun, 2009. **30**(11): p. 846-53.
20. Matsutomo, N., et al., *Optimization of iterative reconstruction parameters with 3-dimensional resolution recovery, scatter and attenuation correction in ^{123}I-FP-CIT SPECT.* Ann Nucl Med, 2015. **29**(7): p. 636-42.
21. Booij, J., et al., *The clinical benefit of imaging striatal dopamine transporters with [123I]FP-CIT SPET in differentiating patients with presynaptic parkinsonism from those with other forms of parkinsonism.* European journal of nuclear medicine, 2001. **28**: p. 266-72.
22. Winz, O.H., et al., *Image quality and data quantification in dopamine transporter SPECT: advantage of 3-dimensional OSEM reconstruction?* Clin Nucl Med, 2012. **37**(9): p. 866-71.
23. Khorshidi, A., *Assessment of SPECT images using UHRFB and other low-energy collimators in brain study by Hoffman phantom and manufactured defects.* The European Physical Journal Plus, 2020. **135**(2): p. 261.
24. Van Laere, K., et al., *Nonuniform transmission in brain SPECT using 201Tl, 153Gd, and 99mTc static line sources: anthropomorphic dosimetry studies and influence on brain quantification.* J Nucl Med, 2000. **41**(12): p. 2051-62.
25. Matsuda, H., et al., *Correction for partial-volume effects on brain perfusion SPECT in healthy men.* J Nucl Med, 2003. **44**(8): p. 1243-52.
26. Biggans, T.J., *Same day cerebral perfusion and dopamine transporter imaging for differential diagnosis of cerebral impairment.* Med Eng Phys, 2019. **64**: p. 56-64.

27. Seret, A. and J. Forthomme, *Comparison of different types of commercial filtered backprojection and ordered-subset expectation maximization SPECT reconstruction software.* J Nucl Med Technol, 2009. **37**(3): p. 179-87.

Figures

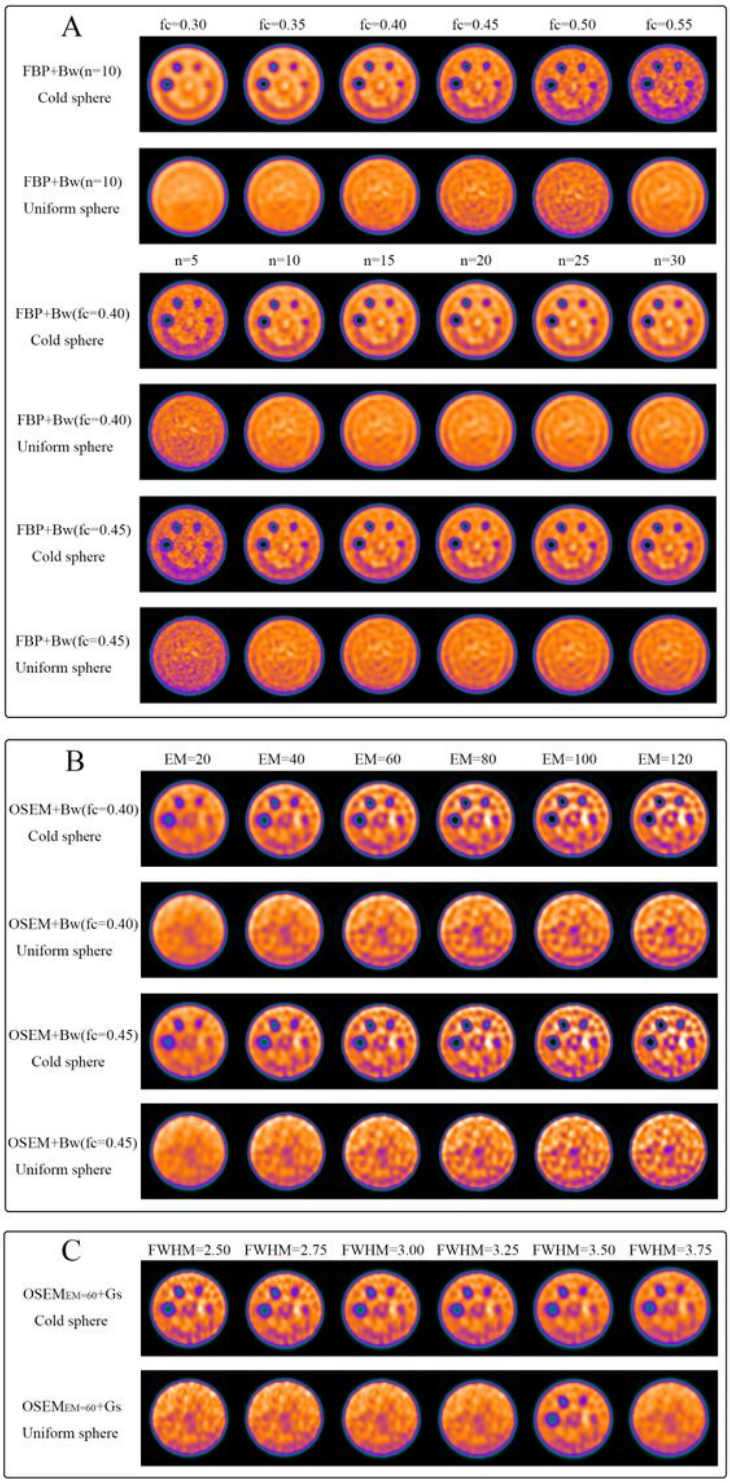

Figure 1

The cross-sectional images of the cold and uniform areas obtained by the FBP+Bw reconstruction method (a): the first and second rows were n=10, and fc values from left to right were 0.30, 0.35, 0.40, 0.45, 0.50, and 0.55 in sequence. The 3rd to 6th rows were fc=0.40 or 0.45, and n values from left to right were 5, 10, 15, 20, 25, and 30 in sequence. The cross-sectional images of the cold and uniform areas were obtained by the OSEM+Bw reconstruction method (b): from left to right EM was 20, 40, 60, 80, 100, and 120 in sequence. The cross-sectional images of the cold and uniform areas obtained by the OSEM+Gs reconstruction method (c): from left to right the FWHM values were 2.50, 2.75, 3.00, 3.25, 3.50, and 3.75 mm in sequence.

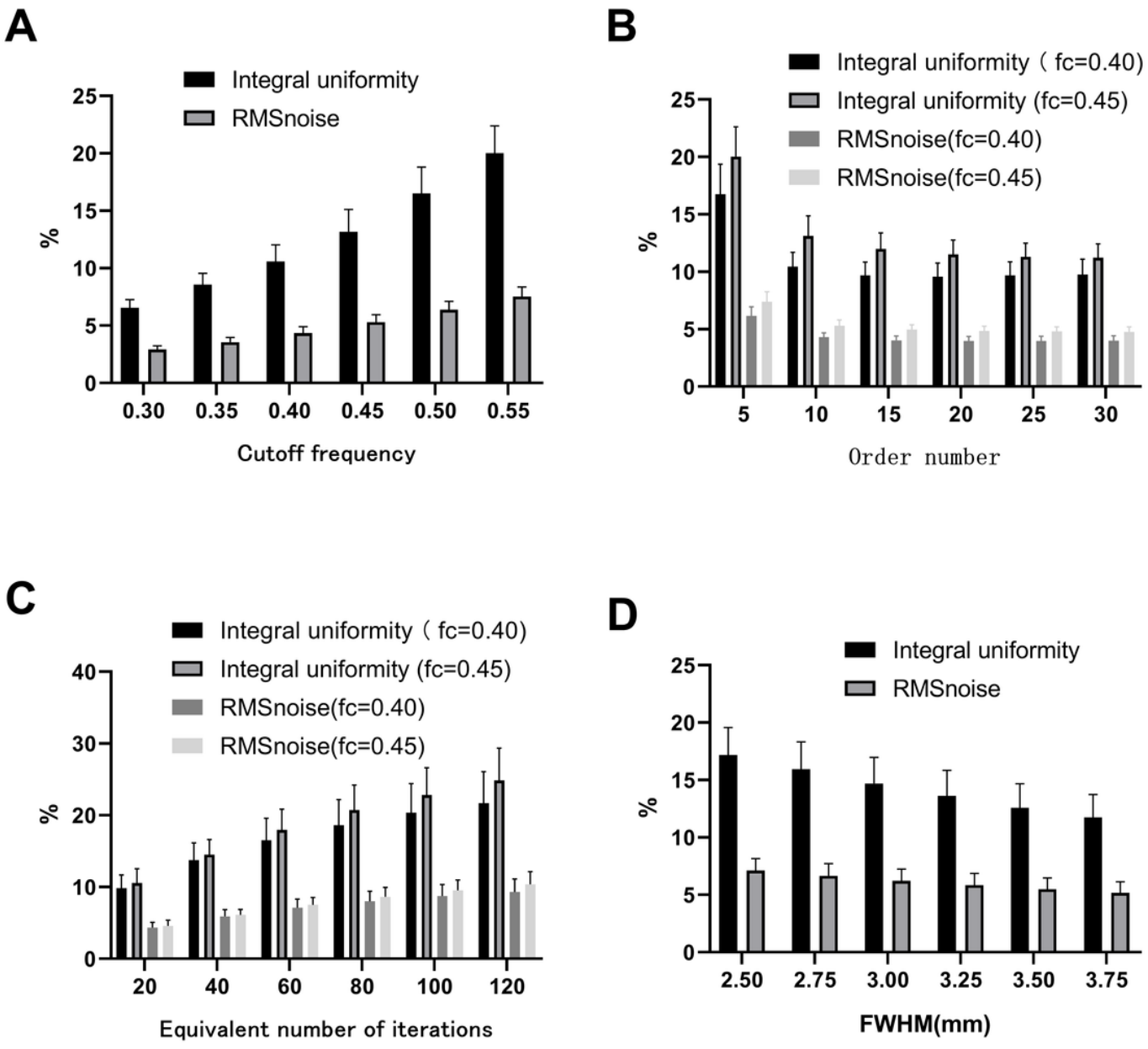

Figure 2

FBP+Bw, n=10, integral uniformity, and RMS noise of the phantom image at different fc values (a). FBP+Bw, fc=0.40 or 0.45, the integral uniformity, and RMS noise of the phantom image at different n

values (b). OSEM+Bw, EM=60, integral uniformity, and RMS noise of the phantom image under different EM values (c). OSEM+Gs, EM=60, integral uniformity, and RMS noise of the phantom image under different FWHM values (d).

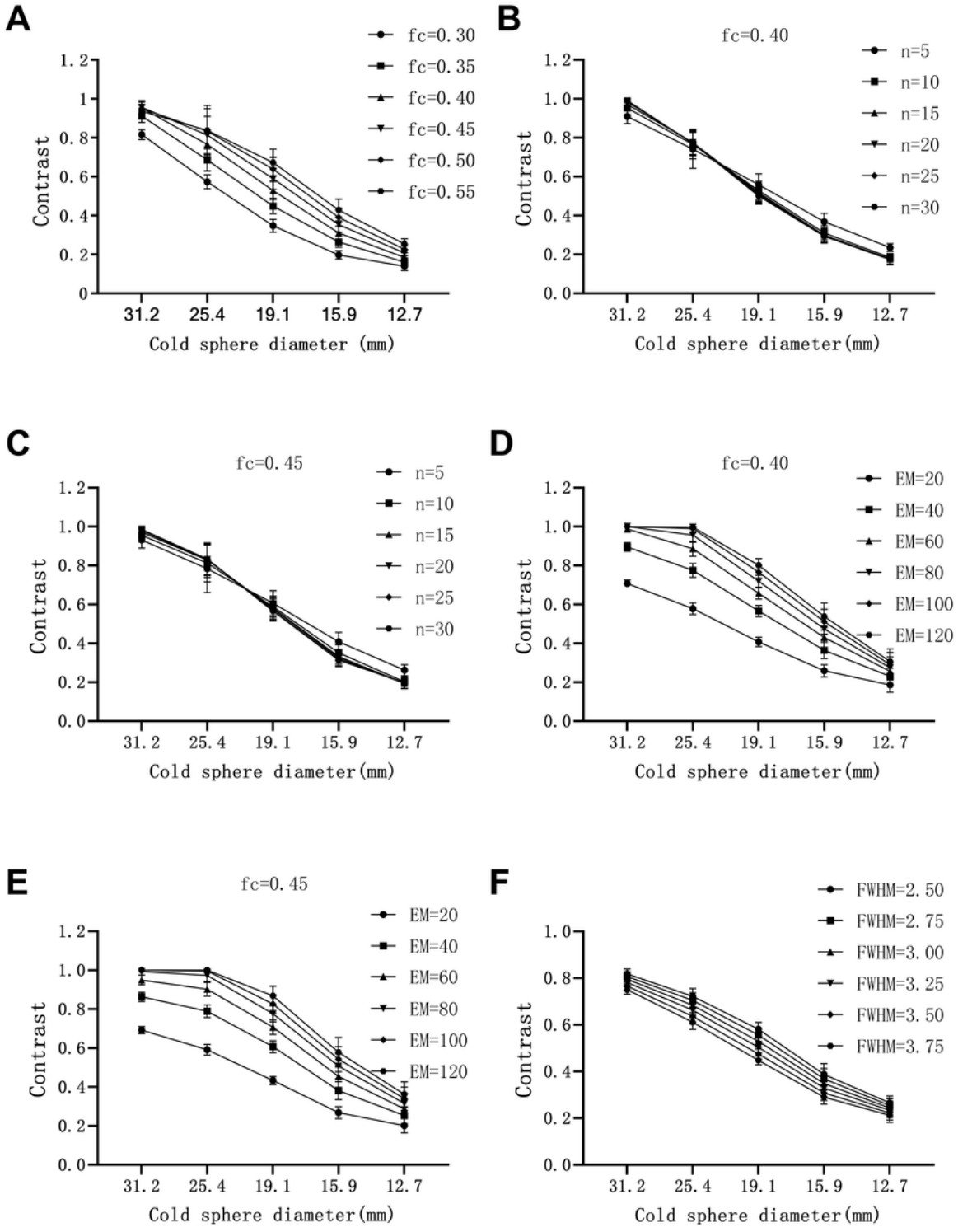

Figure 3

FBP+Bw, n=10, the contrast of cold areas of different sizes in the phantom image at different fc values (a); FBP+Bw, fc=0.40, the contrast of cold areas of different sizes in the phantom image at different n

values (b); FBP+Bw, fc=0.45, the contrast of cold areas of different sizes in the phantom image at different n values (c); OSEM+Bw, fc=0.40, the contrast of cold areas of different sizes in the phantom image at different EM values (d); OSEM+Bw, fc=0.45, the contrast of cold areas of different sizes in the phantom image at different EM values (e); OSEM+Gs, EM=60, the contrast of cold areas of different sizes in the phantom image at different FWHM values (f).

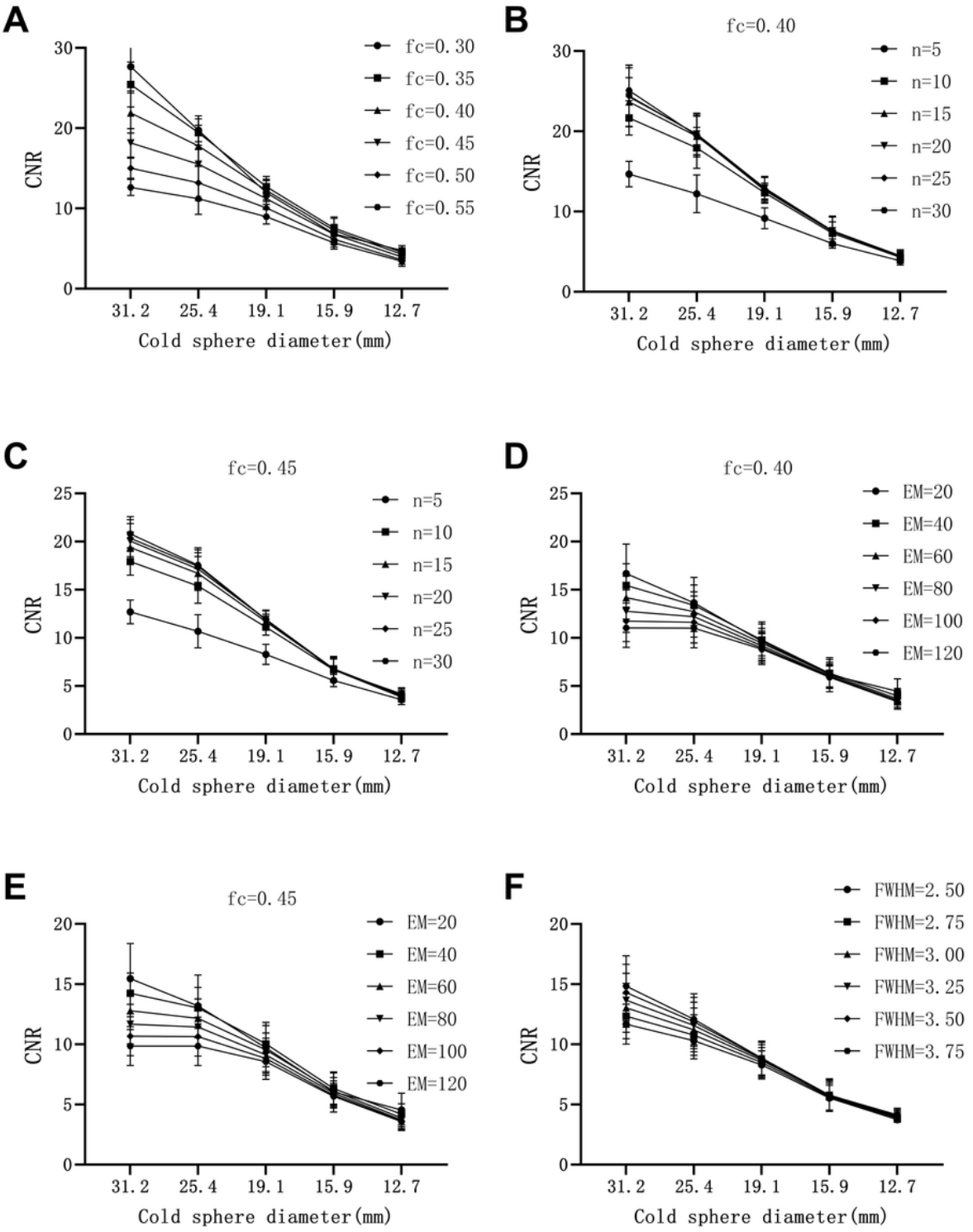

Figure 4

FBP+Bw, n=10, the CNR of cold areas of different sizes in the phantom image at different fc values (a); FBP+Bw, fc=0.40, the CNR of cold areas of different sizes in the phantom image at different n values (b); FBP+Bw, fc=0.45, the CNR of cold areas of different sizes in the phantom image at different n values (c); OSEM+Bw, fc=0.40, the CNR of cold areas of different sizes in the phantom image at different EM values (d); OSEM+Bw, fc=0.45, the CNR of cold areas of different sizes in the phantom image at different EM values (e); OSEM+Gs, EM=60, the CNR of cold areas of different sizes in the phantom image at different FWHM values (f).

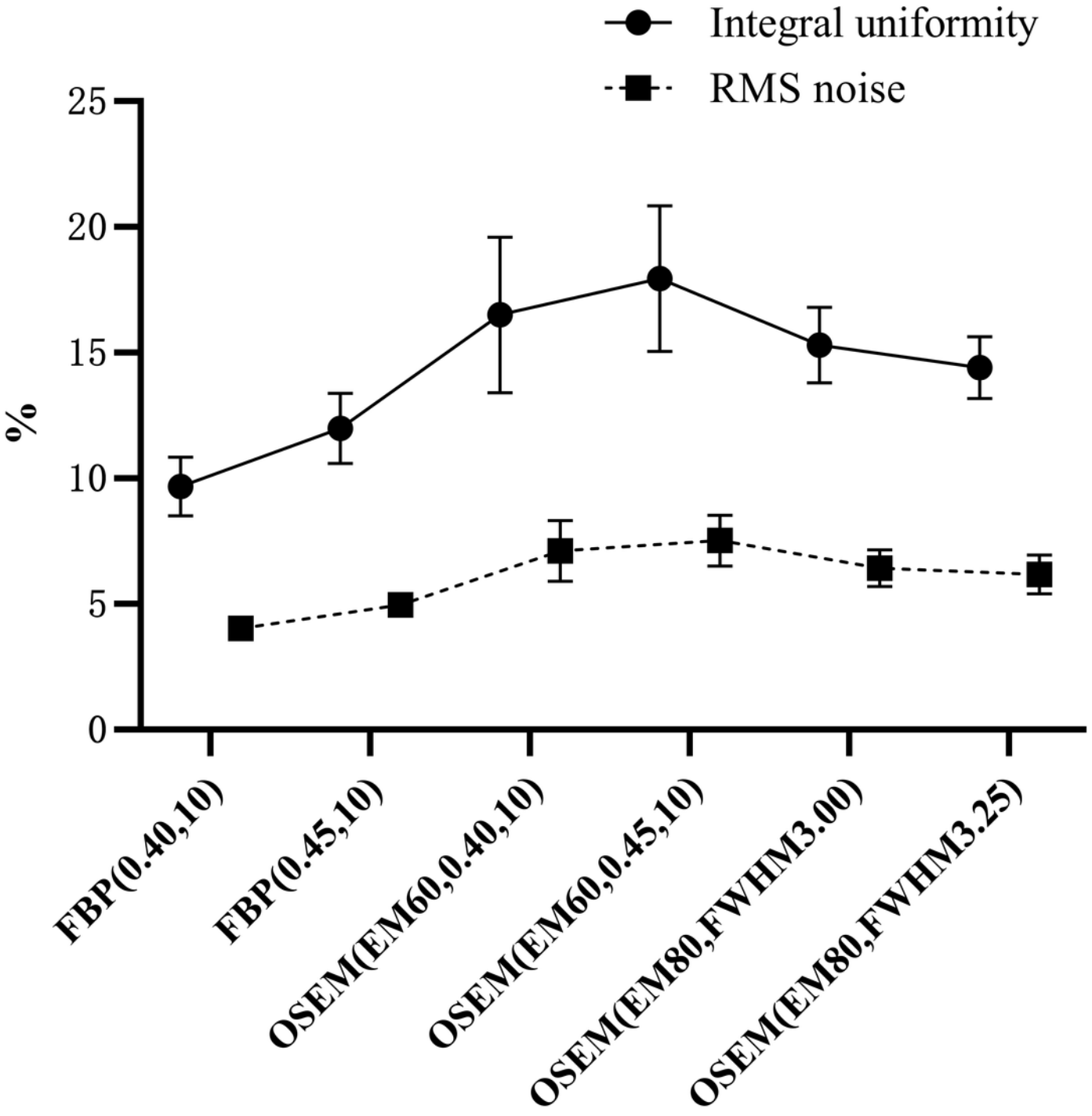

Figure 5

The curves of integral uniformity and RMS noise of the phantom image after processing the best parameters of the three reconstruction combinations.

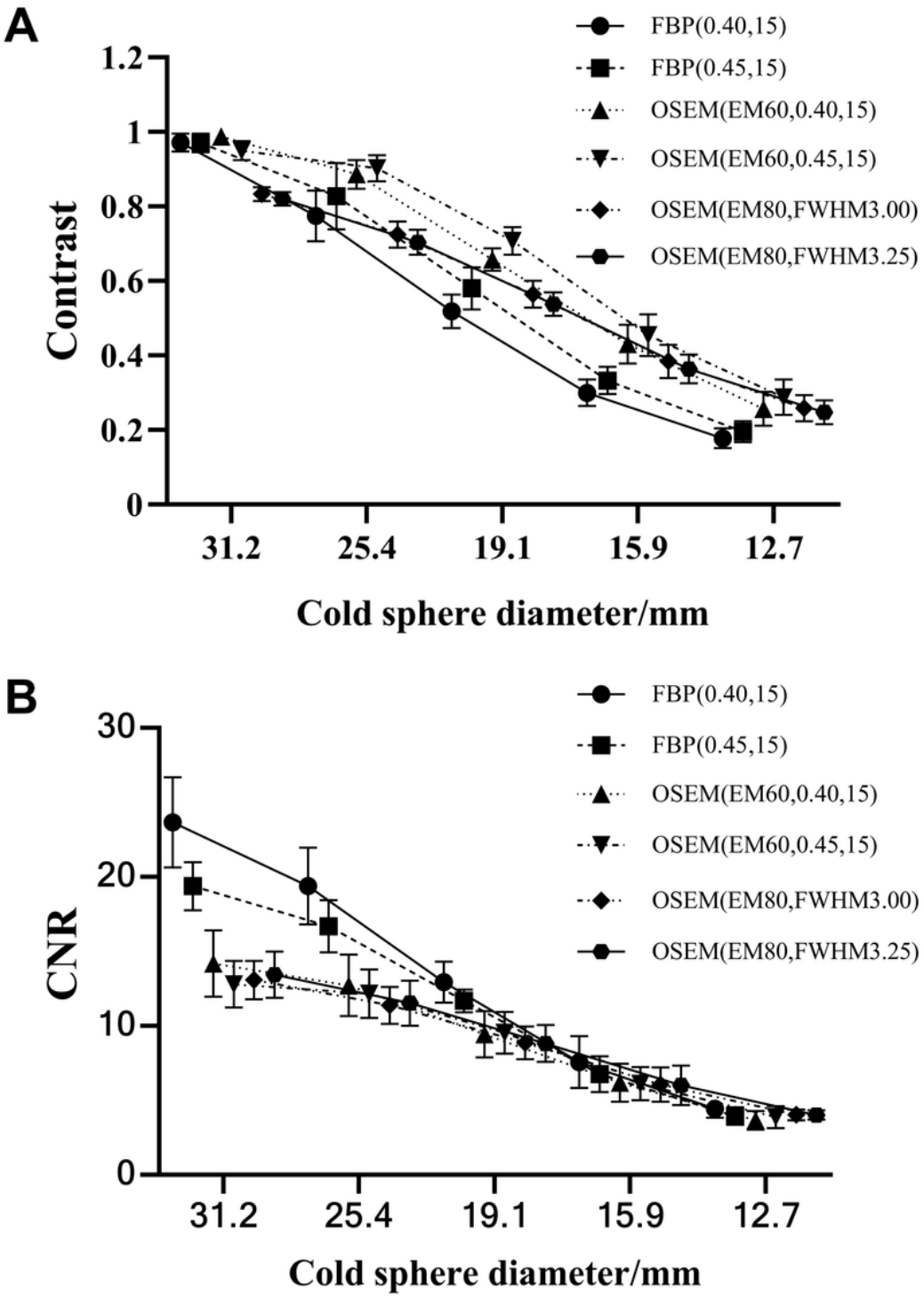

Figure 6

The curve of the contrast of the phantom image after the best parameter processing of the three reconstruction combinations (a). The curve of the CNR of the phantom image after processing the best parameters of the three reconstruction combinations (b).

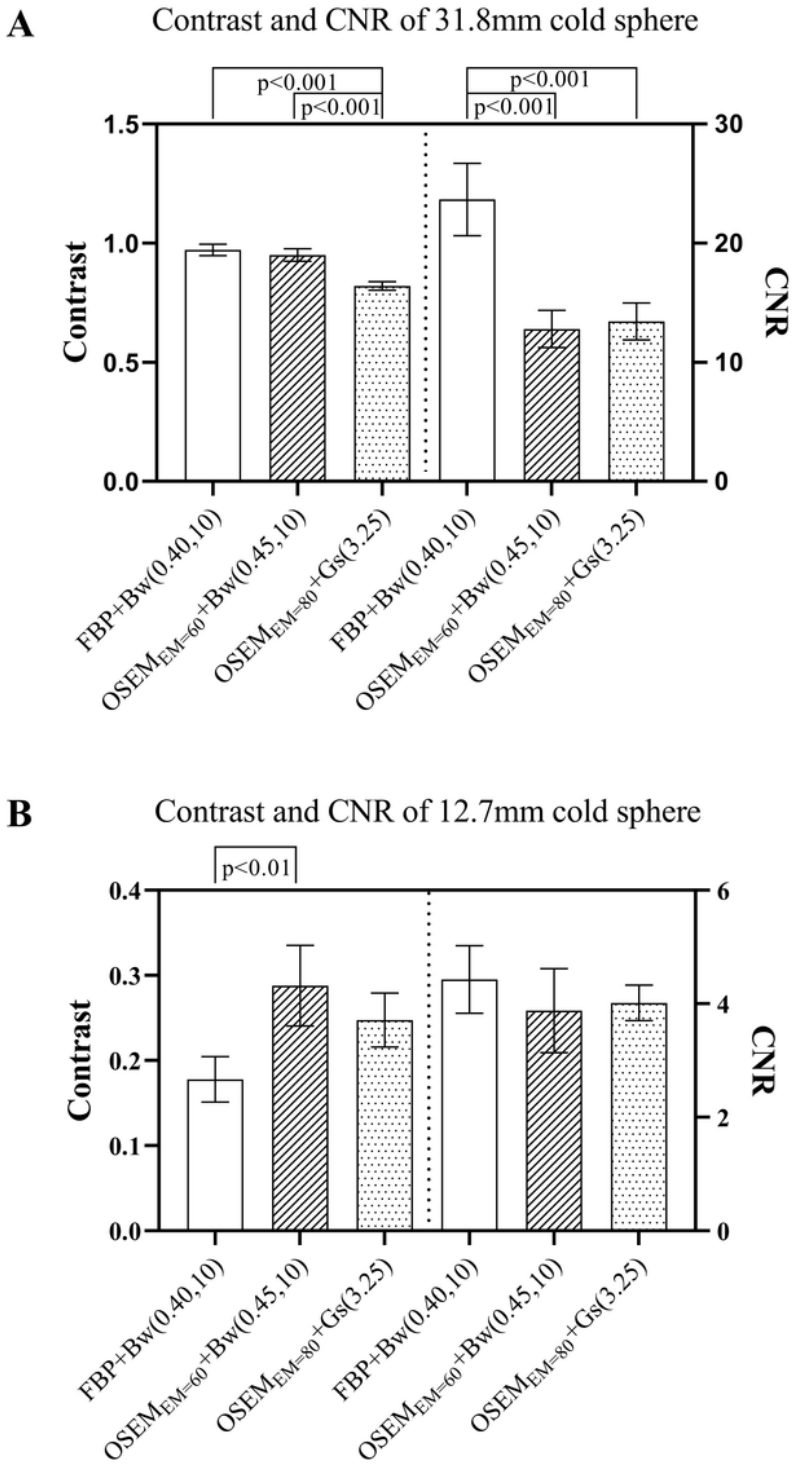

Figure 7

The contrast and CNR of a cold sphere with a diameter of 31.8 mm (a) and a cold sphere with a diameter of 12.7 mm (b) after processing the best parameters of the three reconstruction combinations.

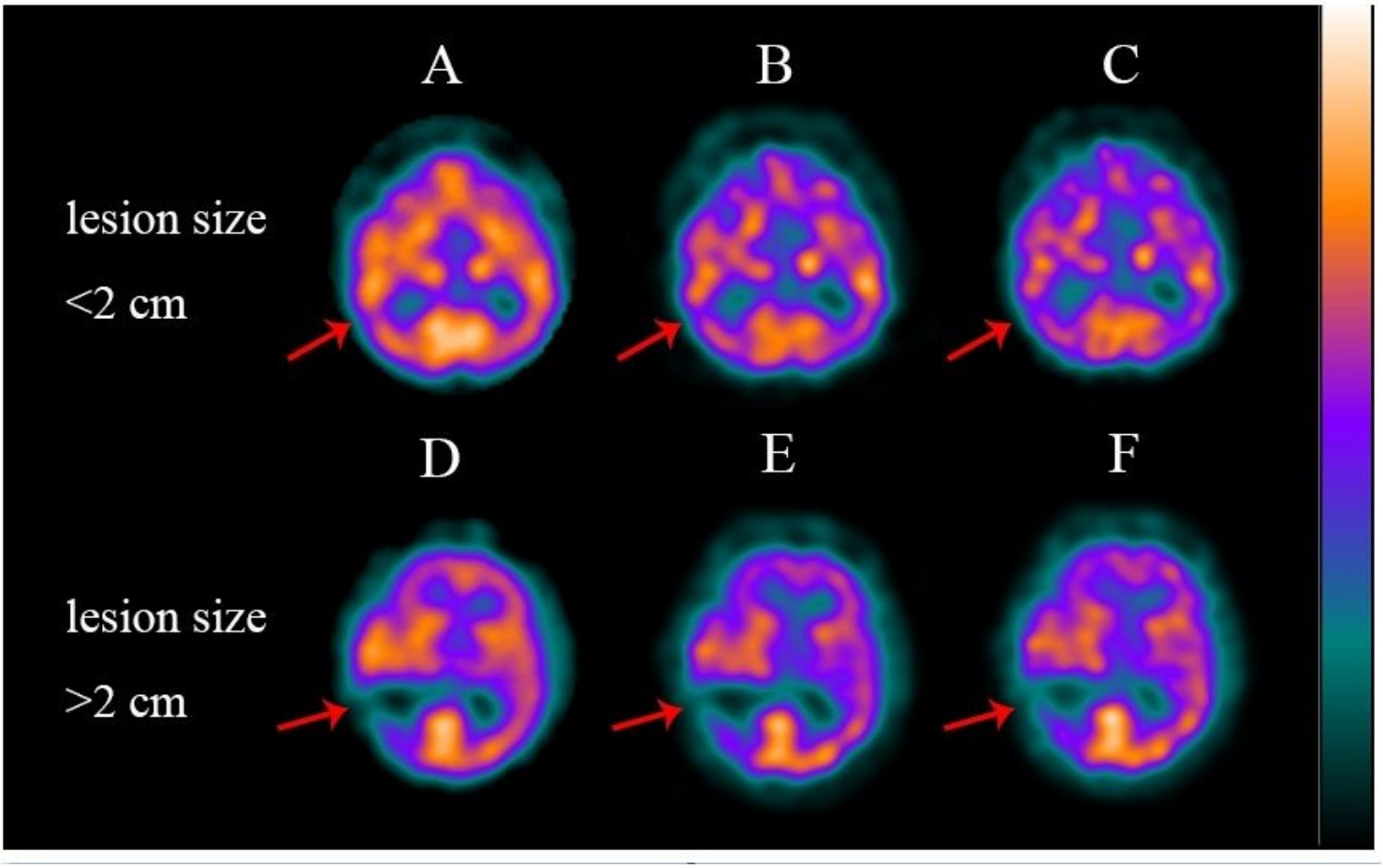

Figure 8

Images of patients with lesion size <2 cm reconstructed using three methods: FBP+Bw (fc=0.40, n=10) (a), OSEM+Bw (EM=60, fc=0.45, n=10) (b), and OSEM+Gs (EM=80, FWHM=3.25) (c). Images of patients with lesion size ≥2 cm reconstructed using three methods: FBP+Bw (fc=0.40, n=10) (d), OSEM+Bw (EM=60, fc=0.45, n=10) (e), and OSEM+Gs (EM=80, FWHM=3.25) (f).